npj | clean water

Article

Published in partnership with King Fahd University of Petroleum & Minerals

https://doi.org/10.1038/s41545-024-00328-3

Reusable and effective polyacrylic membranes for mecoprop and bentazon extractions

Gianluca Utzeri[1,4], José Carlos Guirado-Moreno[1,2,4], Tânia F. G. G. Cova[1], Alberto A. A. C. Pais[1], Luis A. E. Batista De Carvalho[3], Saturnino Ibeas[2], José M. García[2], Artur J. M. Valente[1] ✉ & Saúl Vallejos[1,2] ✉

This study introduces reusable polyacrylic membranes, fabricated from commercially available monomers (1-vinyl-2-pyrrolidone and methylmethacrylate), as a promising approach for pesticide extraction. These membranes effectively remove the commonly used herbicides mecoprop (RE ≈ 99%) and bentazon (RE ≈ 95%) at low concentrations, which pose water contamination risks due to their water-soluble properties and leaf-level sorption. The membranes exhibit excellent manageability and resistance, allowing for safe handling without personal protective equipment. Additionally, the material is environmentally friendly and can be washed and reused for at least 4 cycles without a significant decrease in performance. Characterization techniques, including NMR, TGA, DSC, mechanical testing, N2 adsorption, and FTIR analysis, were used to investigate properties and assess the influence of the polymeric composition. The study focused on examining the lateral charged aminoethyl groups, which play a crucial role in sorbent-sorbate interactions. Sorption kinetics, isotherms, and permeation studies provided insights into the removal mechanism, efficiency, and permeability coefficients, revealing hydrophobic–hydrophobic interactions between the pesticides and the polymer. Molecular dynamics simulations revealed a scorpion-like conformation of the macromolecular chains surrounding the pesticides. These findings support the hydrophobic nature of the extraction mechanism and highlight the significant role of charged aminoethyl groups in facilitating this process.

Water-soluble active agrochemical ingredients can be readily mixed and applied as aqueous commercial pesticide formulations. These formulations are utilized for pre- or post-emergence pest management in agricultural, ornamental, and sports fields to control various types of pests. The term "pesticide" encompasses insecticides, fungicides, herbicides, molluscicides, repellents, biocides, and growth regulators[1]. The utilization of water-soluble pesticides offers several advantages, such as rapid sorption by plants and pests through systemic or passive mechanisms, resulting in a narrow or broad spectrum of action[2].

The drawback of high solubility is the heightened probability of mobility through runoff and leaching in the soil, ultimately reaching water streams[3]. Therefore, the implementation of pest management practices (IPM), which involve appropriate timing, dosage, and selection of suitable formulations, is crucial and strongly advocated to mitigate potential adverse impacts on ecosystems[4].

Mecoprop (MCP) and bentazon (BTZ) are water-soluble active ingredients applied as post-emergence herbicides that exhibit sorption at the leaf level. MCP acts systemically as a growth regulator, while BTZ inhibits photosynthesis in plants, causing them to starve and eventually die[5].

MCP is a neurotoxic phenoxypropionic herbicide commonly employed in non-crop areas for the management of broadleaf weeds in

[1]CQC-IMS, Department of Chemistry, University of Coimbra, 3004-535 Coimbra, Portugal. [2]Grupo de Polímeros, Departamento de Química, Facultad de Ciencias, Universidad de Burgos, Plaza de Misael Bañuelos s/n, 09001 Burgos, Spain. [3]Molecular Physical-Chemistry R&D Unit, Department of Chemistry, University of Coimbra, 3004-535 Coimbra, Portugal. [4]These authors contributed equally: Gianluca Utzeri, José Carlos Guirado-Moreno. ✉e-mail: avalente@ci.uc.pt; svallejos@ubu.es

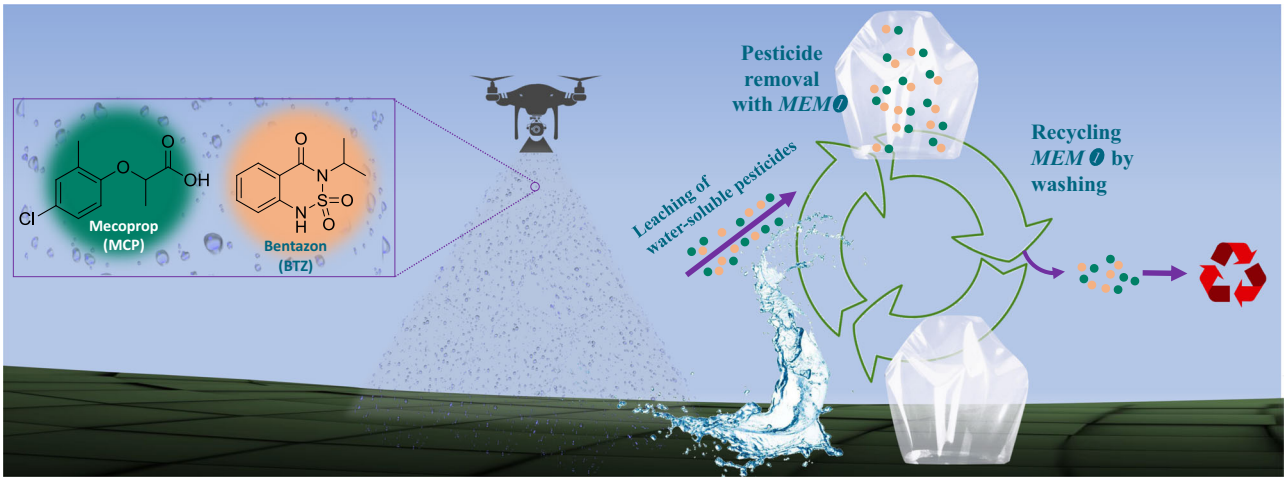

Fig. 1 | Graphical abstract of the study.

lawns, golf courses, and other turfgrass areas. It is classified as a hazardous substance. Furthermore, there have been reports suggesting a link between MCP exposure and an elevated risk of developing non-Hodgkin's lymphoma, a type of cancer that affects the lymphatic system[6].

On the other hand, BTZ is a benzothiazinone herbicide commonly utilized as a spray to manage a wide range of weeds in various crops, including soybeans, peanuts, and corn. BTZ exhibits persistence in aqueous environments and displays moderate toxicity to birds and aquatic fauna[7].

As previously mentioned, MCP and BTZ exhibit relatively high mobility in soil, with half-life degradation rates (expressed as DT_{50}) of 6.1 and 3.8 days in acidic soils, and DT_{50} of 1.9 and 4.9 days in calcareous soils, respectively[8]. Several studies have revealed the concerning presence of these pesticides in women's hair[9], and various natural environments, including the Ebro river delta in Spain[10,11], as well as different effluents from European treatment plants[12]. These findings emphasize the alarming nature of these toxic compounds.

In this study, we present a novel material composed of 100% commercial monomers that offers an efficient extraction method for these two pesticides. The membrane-shaped material is characterized by excellent manageability and durability, eliminating the need for personal protective equipment (PPE) during usage. Additionally, it is reusable and environmentally friendly, as illustrated in Fig. 1, as it can be washed and reused. The scalability of this material makes it easily adaptable for large-scale applications.

The influence of polymeric composition and the presence of lateral charged aminoethyl groups on the membrane properties and sorption performance of BTZ and MCP is investigated. The polymeric membranes were subjected to comprehensive characterization using various techniques, such as NMR, thermogravimetric analysis (TGA), differential scanning calorimetry (DSC), mechanical testing, N2 adsorption, and Fourier-Transform infrared spectroscopy.

The sorption kinetics, isotherms, and permeation were conducted to determine the sorption mechanism, removal efficiency, and permeability coefficients, providing insights into the interactions between the pesticide and polymer, as well as their corresponding mechanisms. The performance of the polymeric materials was also tested in the presence of nitrogen fertilizers as interfering substances. Additionally, explicit water molecular dynamics simulations (MD) were performed to investigate the sorption behavior of bentazon and mecoprop in solution at the molecular level. These simulations included a description of the binding enthalpies and stabilizing/destabilizing noncovalent interactions (NCI). The sorption behavior was studied using a co-polymeric membrane consisting of 1-vinyl-2-pyrrolidone (VP), methyl methacrylate (MMA), 2-(methacryloyloxy)-ethan-1-aminium, and ethylene glycol dimethacrylate (E). A reference membrane without the lateral protonated amino group was also used for comparison.

FTIR and NMR analyses were also performed before and after the interaction with both active ingredients to support, confirm, and enhance the understanding of the sorption studies and molecular dynamics simulation results.

Methods

Materials

All materials and solvents were commercially available and used as received unless otherwise stated. The following materials and solvents were used: 1-vinyl-2-pyrrolidone (VP) (Aldrich, 99%), methylmethacrylate (MMA) (Aldrich, 99%), 2-isocyanatoethyl methacrylate (NCO) (Aldrich, 98%), ethylene glycol dimethacrylate (E) (97.5%, Aldrich), mecoprop (MCP, Aldrich, 99.9%), bentazone (BTZ, Aldrich, 99.9%), urea (Fragon, 100%), ammonium nitrate (Chem-Lab, <99%), distilled hexane (VWR, 99%), 1,4-dioxane (VWR, 100%). Azo-bis-isobutyronitrile (AIBN, Aldrich, 99%) was recrystallized twice from methanol.

Instrumentation and methods

The thermal characterization of the polymers was performed by thermogravimetric analysis (Q50 TGA analyzer, TA Instruments, New Castle, DE, USA) under nitrogen atmosphere at 10 °C·min^{-1}, and by differential scanning calorimetry under a nitrogen atmosphere at a heating rate of 20 °C·min^{-1} (Q200 DSC analyzer, TA Instruments, New Castle, DE, USA), using 10–15 mg of sample for each.

The water uptake capacity of the films upon soaking in pure water at 20 °C until reaching equilibrium (water-swelling percentage, WSP) was obtained from the weight of a dry sample film (ω_d) and its water-swollen weight (ω_s) using the following expression: $WSP = 100 \times [(\omega_s \times \omega_d)/\omega_d]$.

Tensile properties analysis, with 5 × 9.44 × 0.103 mm samples tested at 5 mm min^{-1} (EZ Test Compact Table-Top Universal Tester, Shimadzu Kyoto, Japan).

The active surface area (S_{BET}), pore volume and pore size distribution were determined by nitrogen sorption–desorption analysis (*ASAP 2000, Micrometrics*) for the membrane at 10% of NCO groups before and after washing step in water.

Fourier transform infrared spectra (FTIR) of the prepared polymeric membranes with 1%, 5%, and 10% of the functional monomer before (MEM_1, MEM_5, *and* MEM_{10}, respectively) and after washing step with distilled water (*MEM*❶, *MEM*❺, *and MEM*❿, respectively), were recorded with an infrared spectrometer (FT/IR-4200, Jasco, Tokyo, Japan) with an ATR-PRO410-S single reflection accessory, for full characterization of membranes structure. To better understanding the sorbent-sorbate interaction, additional experiments were carried out with MEM_{10}, before and after dipping on BTZ and MCP aqueous solutions at 50 mg L^{-1}. These spectra were acquired in attenuated total reflectance (ATR) mode, in the

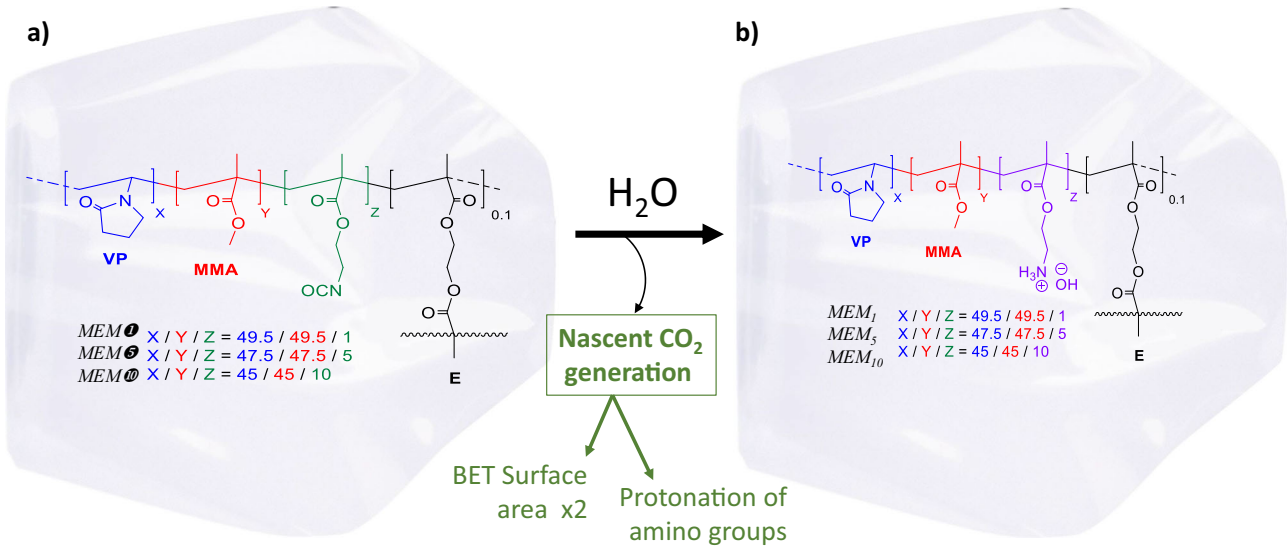

Fig. 2 | Schematic representation of the prepared materials. a Original membranes with isocyanate side groups; and **b** membranes with amino side groups protonated by the nascent carbon dioxide generated after the reaction of the isocyanate groups with water.

mid-IR range (400–4000 cm^{-1}), in a Bruker Optics Vertex 70 FTIR spectrometer purged by CO_2-free dry air and equipped with a Bruker Platinum ATR single reflection diamond accessory. A Ge on KBr substrate beam splitter and a liquid nitrogen-cooled wide band mercury cadmium telluride (MCT) detector were used. Spectra were averaged over 128 scans at a resolution of 2 cm^{-1}, and the 3-term Blackman-Harris apodization function was applied. The Bruker OPUS–Spectroscopy Software (8.1 version) was used to correct the spectra regarding the wavelength dependence of the penetration depth of the electric field in ATR, using a mean refractive index of 1.25.

^{1}H and $^{13}C\{1H\}$ NMR spectra (Advance III HD spectrometer, Bruker Corporation, Billerica, Massachusetts, USA) were recorded at 300 MHz for ^{1}H and 75 MHz for ^{13}C using deuterated dimethyl sulfoxide (DMSO-d_6) at 25 °C as solvent. The experimental conditions for the interaction study between the polymer and MCP are deeply depicted in Section 2.7.

Synthesis of the polymers MEM and POL

Membrane-shaped polymers were prepared by bulk radical polymerization of the monomers VP, MMA, and NCO at different molar ratios, using 0.1 mol% of E as crosslinking, following the experimental procedure described below. In previous stages, the type of monomers, molar ratios, thickness, and degree of crosslinking of the material were optimized to ensure manageability and an appropriate water swelling percentage, while always maintaining the pesticide extraction property, which is the primary objective of the material.

For the membrane labeled as MEM_1 (1 mol% of NCO monomer), 850 mg (7.64×10^{-3} mol) of VP, 765 mg (7.64×10^{-3} mol) of MMA, 24.0 mg (1.54×10^{-4} mol) of NCO, 3.1 mg (1.67×10^{-5} mol) of E were mixed in a test tube. For membranes MEM_5 and MEM_{10}, the corresponding amounts were used to obtain 5 and 10 mol% of NCO, respectively (MEM_5: 800 mg of VP, 719.8 mg of MMA, 117.5 mg of NCO, and 3 mg of E. MEM_{10}: 750 mg of VP, 674.8 mg of MMA, 232.7 mg of NCO, and 2.97 mg of E). To the three mixtures, 18.2 mg (1.1×10^{-4} mol) of AIBN were added and the solution of comonomers and initiator were injected in a mold ($90 \times 120 \times 0.1$ mm, width, length, thickness) comprised between two silanized glasses in an oxygen-free atmosphere[13–15]. The polymerization was carried out at 60 °C, overnight, and finally, the membranes were washed with water to generate aminoethyl groups containing MEM_1, MEM_5 and MEM_{10}. (To refer to the unwashed membranes with NCO groups, we will use the nomenclature *MEM❶, MEM❺, and MEM❿*). The resulting CO_2, produced from NCO groups, dissolves in water immediately causing the protonation of the amine groups, as schematically depicted in Fig. 2. The materials were ultimately die-cut into 8 mm discs using a punch.

Herein, membranes are an excellent working tool, but their crosslinked state prevents their characterization by, for example, liquid-state NMR. Therefore, a representative soluble linear polymer was synthesized to perform further characterizations. The linear polymer (POL_{10}) has the same chemical composition as its respective membrane (MEM_{10}), except for the crosslinking agent, which was not included in the formulation. The monomers and AIBN were dissolved in dioxane at a concentration of 2 mol dm^{-3} (sum of all monomers) and 0.1 mol dm^{-3}, respectively. The solution was heated overnight at 60 °C, and finally precipitated in hexane. The white solid was purified in a Soxhlet using hexane as solvent, and finally dipped in water to generate lateral aminoethyl groups containing polymer (POL_{10}).

The complete physicochemical characterization of all polymers can be found in the Supplementary Material (Supplementary Fig. 1).

Pesticide removal efficiency

Active ingredient concentrations were quantified by UV-Vis spectroscopy measurements (UV-2600*i* Shimadzu, Germany) in the wavelength range of 600-200 nm. Calibrations were performed in the analytical range 0–50 mg L^{-1} for BTZ and MCP, using the absorbance at λ_{max} = 333 nm and 280 nm, respectively (more information in Supplementary Fig. 9 and Supplementary Table 1). The analysis was performed in duplicate, and the solutions were prepared in Milli-Q ultrapure water.

To maximize the reproducibility of the experimental conditions for the sorption analysis, 8 mm diameter disks were used (area ≈ 50.3 mm^2, volume ≈ 5.03 mm^3, weight ≈ 3.8 mg). Initially, membranes MEM_1, MEM_5, *and* MEM_{10} were tested and compared with a blank membrane (without NCO groups, i.e., 50 mol% of VP, 50 mol% of MMA, 0.1 mol% of E). 1 disk from each material was introduced in hermetic vials, dipped into 2 mL of BTZ and MCP aqueous solutions at 10 mg L^{-1}, thermostated at 25 °C and under shaking at 120 rpm into an incubator, for 24 h to ensure that the system reached equilibrium. Finally, the disc is removed from the bottom of the vial with tweezers, and the solution is measured in the UV–visible spectrophotometer. Analytical solutions not containing the membrane were always used as blank solution for each pesticide concentration to determine the initial concentration.

The sorption capacity of the membranes was assessed in term of amount of sorbed pesticide per gram of sorbent (q_e) and removal efficiency

(*RE*), as calculated by following equations:

$$q_e = \frac{C_0 - C_e}{m} \times V \quad (1)$$

$$RE\% = \frac{C_0 - C_e}{C_0} \quad (2)$$

where q_e (mg g^{-1}) is the amount of pesticide sorbed per gram of sorbent. C_0 and C_e (mg L^{-1}) are the concentrations of pesticide at initial and equilibrium state, respectively, m (g) is the mass of the sorbent and V (L) is the volume of solution.

Transport properties evaluation

The transport properties of BTZ and MCP through MEM_1 were evaluated at the maximum concentration to expedite the process (50 mg L^{-1}). Permeability (P) and apparent diffusion (D_{ap}) coefficients were calculated by time-lag method using a horizontal communicating vessel system with a contact area of 2 cm^2 (Eqs. 3 and 4)[16]. The concentration of the active ingredient in each vessel was measured by UV-Vis spectroscopy, as a function of time, at 25 °C and stirred at 250 rpm.

$$D_{ap} = \frac{L^2}{6\theta} \quad (3)$$

$$P = \left(\frac{V}{A}\right) \times S \times \left(\frac{L}{C_{pesticide}}\right) \quad (4)$$

where L (cm) is the membrane thickness, θ (s) is the time-lag, A (cm^2) is the permeation area, S (mg L^{-1} s^{-1}) is the slope of the flux of permeant as a function of time in steady state conditions and $C_{pesticide}$ (mg L^{-1}) is the initial concentration of pesticide.

The values of D_{ap} and P were used to calculate the apparent coefficient of partition (S_{ap}), which indicates the affinity of the analyte to the membrane, calculated by the following equation:

$$S_{ap} = \frac{P}{D_{ap}} \quad (5)$$

Sorption study

The kinetic sorption analysis was carried out in 2 mL of solution at 10 mg L^{-1} of each pesticide into MEM_1, for 24 h, at 25 °C. The kinetic mechanism was studied from a diffusion point of view by fitting a solution of Fick's 2nd law equation to the experimental data, which considers the system as a plane sheet (Eq. 6):

$$\frac{q_t}{q_e} = 1 - \frac{8}{\pi^2} \sum_{n=0}^{\infty} \frac{1}{(2n+1)^2} \exp\left[\frac{-(2n+1)^2 \pi^2 Dt}{l^2}\right] \quad (6)$$

where q_t (mg g^{-1}) is the amount of sorbed pesticide per gram of sorbent over time, t (s) is the time, l (cm) is half of the thickness of the membrane and D (cm^2 s^{-1}) is the diffusion coefficient. The D value was used to calculate the effective partition coefficient (S), by replacing D_{ap} by D in Eq. (5). The conditions of the Fickian model are that the membrane is at $t = 0$ at uniform concentration C_0 and at time t with one face $x = 0$ at constant concentration C_0 and the other $x = l$, $C_2 = 0$.

Considering the analytical range of concentration, the isotherm analysis was performed in duplicate within 1–50 mg L^{-1} of pesticide solution (2 mL), 24 h, at 25 °C. Langmuir (Eq. 7) and Brunauer–Emmet–Teller (BET) (Eq. 8) models were fitted to the experimental data. The non-linear equations are as following.

$$q_e = \frac{q_m K_L C_e}{1 + K_L C_e} \quad (7)$$

$$q_e = \frac{q_s C_{BET} C_e}{\left(C_s + (C_{BET} - 2)C_e - \left((C_{BET} - 1)\frac{C_e^2}{C_s}\right)\right)} \quad (8)$$

where q_m (mg g^{-1}) is the maximum sorption capacity per weight unit of sorbent and K_L (L mg^{-1}) is the Langmuir constant. q_s (mg g^{-1}), C_{BET} (L mg^{-1}) and C_s (mg L^{-1}) are the theoretical isotherm saturation capacity, BET constant for sorption isotherm and the sorbate monolayer saturation concentration, respectively.

Interactions pesticide–polymer as seen by ^{1}H-NMR

Interactions between MCP and POL_{10} were evaluated by ^{1}H-NMR by using the continuous variation method (the same experiment was conducted with BTZ; however, it did not yield satisfactory results). 11 mg of MCP were dissolved in 0.6 mL of DMSO-d_6, and the first spectrum was recorded as blank. After that, increasing amounts of a solution of POL_{10} (180 mg in 0.8 mL of DMSO-d_6) were added, and the NMR spectra were recorded after each addition. To proceed with the calculations, it is considered that the interaction occurs between MCP and the active centers of the polymers (i.e., monomer units with NH_3^+ groups). Therefore, the concentration of active centers was determined, taking into account that the polymer contains 10 mol% of this monomer. The exact amounts are detailed in Supplementary Table 2.

Given the concentration of the two species (MCP and monomers with NH_3^+ subunits), a Job's plot is constructed (Supplementary Figure 10), revealing that the stoichiometry of the formed complex is 1:1. Based on this, the interaction scheme can be formulated as follows:

$$MCP + POL_{10} \overset{K}{\rightleftharpoons} MCP - POL_{10} \quad (9)$$

By considering the mass balance equation:

$$C_{MCP} = [MCP] + [MCP - POL_{10}] \quad (10)$$

$$C_{POL10} = [POL_{10}] + [MCP - POL_{10}] \quad (11)$$

and from the definition of the equilibrium constant, the following equation is derived, from which the aforementioned constant was calculated.

$$[MCP]_{eq} = C_{MCP} - \frac{1}{2}\left(\left(C_{MCP} + C_{POL10} + \frac{1}{K}\right) - \sqrt{\left(C_{MCP} + C_{POL10} + \frac{1}{K}\right)^2 - 4C_{MCP} * C_{POL10}}\right) \quad (12)$$

Competitive interaction, interference study, and reusability

The selective and the competitive interaction into MEM_1 were tested in aqueous solution of BTZ and MCP at different molar ratio (0.5/1, 1/1, 1/0.5 mol_{BTZ}/mol_{MCP}), and constant total molar concentration of 0.07×10^{-3} mmol dm^{-3}. Additionally, NH_4NO_3 and urea were used as ionic and non-ionic interferents, respectively, on the sorption of pesticides, at different molar ratio within (0.5, 1, 1.5, 2 $mol_{interferent}/mol_{pesticide}$) with BTZ or MCP at 10 mg L^{-1}. Those two compounds were chosen as two examples of the most widely applied class of nitrogen fertilizers, aiming mimetizing their presence in water[17,18]. The reusability of MEM_1 was tested for four sorption/desorption cycles, using 2 mL of aqueous solution of BTZ and MCP at 50 mg L^{-1}, for 24 h at 25 °C. The desorption steps were performed both in distilled water and in NaOH 0.1 mol dm^{-3}. In the latter case, after NaOH washing the membrane is dipped in HCl 0.1 mol dm^{-3}, primarily to remove any traces of NaOH that could hinder the protonation of the membrane in

distilled water, considering that the calculated pKa of the amino group is 8.1[19]. Analysis were performed in duplicate.

In silico rationale for elucidating interaction patterns through molecular dynamics simulations

The specific sorption behavior of MCP and BTZ in solution through the membrane, represented as two simple models containing 5:5:1 monomeric units of VP/MMA/E with (*i*) one protonated amino side group (MEM_{10}), or (*ii*) without this protonated amino side group (*MEM*, used as reference), was investigated by calculating the binding enthalpies underlying the association between MEM_{10} and *MEM* and both pesticides (MEM_{10}:*BTZ*, *MEM*:BTZ, MEM_{10}:MCP, and *MEM*:MCP complexes), and by analyzing the topological features of the electronic charge densities of the interacting molecules (see refs. 20 and [21] for details).

The systems were modeled and simulated using GROMACS software (version 2022.1) using the all-atom Gromos 54a7 force field to describe both membrane polymer and pesticide molecules in the presence of explicit water molecules. The binding partners were first placed in a vacuum environment, and their initial coordinates were set according to their respective starting conformations.

The binding enthalpies were calculated from the following equation:

$$\Delta H = \langle H \rangle_{MEM:BTZ/MCP} + \langle H \rangle_{pure\ water} - \langle H \rangle_{MEM} - \langle H \rangle_{BTZ/MCP} \quad (13)$$

where $\langle H \rangle MEM{:}BTZ/MCP$, $\langle H \rangle pure\ water$, $\langle H \rangle$ *MEM* and $\langle H \rangle BTZ/MCP$ are the Boltzmann averaged total potential energies for the hydrated MEM_{10}:BTZ, *MEM*:BTZ, MEM_{10}:MCP, and *MEM*:MCP complexes, pure water, and single hydrated MEM_{10}, *MEM*, BTZ and MCP systems, respectively. The intermolecular interactions from MEM_{10} and *MEM* complexes were also characterized in terms of their nature and strength to provide a complementary rationale to the influence of the protonated amino group on membrane structure and performance.

Hydrated MEM_{10}, *MEM*, BTZ and MCP molecules were also considered as system references. For MEM_{10} and *MEM* backbones five units of VP and MMA and one unit of E were considered, in order to achieve the appropriate polymeric composition of the membrane used experimentally.

The starting geometries of MEM_{10}, *MEM* and pesticide molecules were constructed in Avogadro and Pymol and optimized with the semi-empirical Antechamber/SQM method. The topologies for each molecule were generated using the Automated Topology Builder server (version 3.0) and partial charges for each molecule were obtained from the semi-empirical (AM1) with bond charge correction (BCC) method[22].

To obtain the initial binding states for the hydrated systems, vacuum simulations (20 ns) were performed. These simulations provided insights into the initial binding state and interaction patterns between MEM_{10}, *MEM* and each pesticide. Understanding the initial conformational preferences and intermolecular interactions in this simplified environment guided the setup of subsequent hydrated simulations. During the production run, the binding partners were allowed to explore the conformational space without solvent effects. The simulation boxes were defined with sufficient dimensions to accommodate the binding partners, ensuring an appropriate buffer space around them.

For the simulations in water, a cubic box of 5.5 nm edge-length was used for each system containing one single hydrated MEM_{10}, *MEM*, BTZ, and MCP molecule or one molecule of each binding pair (corresponding to the initial binding states of MEM_{10}:BTZ, *MEM*:BTZ, MEM_{10}:MCP, and *MEM*:MCP complexes obtained from vacuum simulations), solvated with explicit SPC216 water molecules.

The energy minimization was performed to remove any steric clashes or unfavorable contacts within the systems. Following energy minimization, a constant temperature and pressure of 300 K and 1 bar, respectively, were imposed in all simulations, by the coupling constants of 0.1 ps and 2 ps, to V-rescale and Berendsen external baths. A standard time step of 2 fs was used for both equilibration and production runs. Nonbonded interactions were computed based on a neighbor list, updated every 10 steps. Lennard–Jones interactions and electrostatic interactions were computed using a cut-off of 1.2 nm and the particle mesh Ewald (PME) method, respectively. The constraints in the binding partners were imposed by the LINCS algorithm. The equilibration phase involved restraining the polymer with position constraints while allowing the other system components to equilibrate. This allowed the binding partners to adjust to the water environment and attain a stable conformation.

Molecular dynamics (MD) simulations were conducted in a periodic boundary condition setting, encompassing all three dimensions (*x*, *y*, and *z*)[23,24]. Equilibrium properties, structural characteristics, and dynamics of *MEM* systems were computed over 200 ns simulation runs subsequent to a 50 ns equilibration period. Throughout the equilibration phase, the box dimensions remained constant by employing position restraints on the box, effectively constraining bond lengths during the simulation. Notably, no pressure coupling was applied during the production runs, ensuring the preservation of the simulation box size[20,23].

Sufficient simulated time (200 ns) was allocated to obtain a reliable statistical dataset for the binding enthalpies, and the final 50 ns of the simulations were subjected to standard analyses. These analyses encompassed various parameters, including the time-dependent root mean square deviation (RMSD) calculations for both MEM_{10} and *MEM* atoms in their free states and upon binding to BTZ and MCP. Furthermore, the coordination number of water molecules surrounding specific groups of the binding partners was determined by integrating the area under the radial distribution function (RDF) curve, determining the number of polymer-water and pesticide-water molecule interactions within a certain distance. Additionally, a geometric clustering algorithm based on a hierarchical (top-down) approach, as outlined in[25], was employed to identify and categorize structurally similar conformations sampled during the MD simulations. This clustering analysis facilitated the assessment of the prevalence of each MEM_{10} and *MEM* structure and aided in the selection of representative complex conformations for further analysis using the IGM method.

Analysis of noncovalent interactions by IGM

The analysis of noncovalent interactions (NCI) was performed using the Independent Gradient Method (IGM)[23], which allows the visualization of regions of low charge density corresponding to stabilizing/destabilizing NCI based on the analysis of the electronic charge density of the interacting molecules and their gradients, as well as the quantitative comparison of the strength of NCI interactions by calculating the IGM descriptor δg, which directly corresponds to the charge density gradient(s) in real space[20,23,26].

The analysis of the electronic charge density and its gradients in the binding partners was conducted using the IGMPlot software (version 3.0). This software facilitated the visualization and quantification of specific regions associated with noncovalent interactions that either stabilize or destabilize the complexes. The IGM method employed in this analysis is based on the topological properties of the electronic charge density (ρ) and utilizes quantities derived from the first and second derivatives of the density. To obtain the IGM descriptor, δg^{inter}, the first derivatives of the charge densities for the final complexes were compared with those of the respective free components.

$$\delta g^{inter} = \left|\nabla \rho^{IGM,inter}\right| - \left|\nabla \rho\right| \quad (14)$$

The nature and strength of NCI are detected when δg^{inter} takes positive values and the size of the descriptor is determined at a point in space. The term $\nabla \rho^{IGM,inter}$ is calculated from the sum of the N atoms in the two binding partners (A and B) along the x-direction,

$$\left(\frac{\delta_\rho}{\delta_x}\right)^{IGM,inter} = \left|\sum_{i=1}^{N_A} \frac{\delta_{\rho_i}}{\delta_x}\right| + \left|\sum_{i=1}^{N_B} \frac{\delta_{\rho_i}}{\delta_x}\right| \quad (15)$$

The visualization of non-covalent interactions was also performed using IGMPlot software, which utilizes precomputed atomic charge

densities to estimate a pro-molecular density with minimal impact on these interactions. While δg^{inter} serves the purpose of identifying NCI regions, ∇^2_ρ, the second Laplacian derivative of the density, is employed to distinguish between stabilizing and destabilizing non-covalent interactions. By decomposing ∇^2_ρ into its three eigenvalues (λ) that exhibit maximal variation, $\nabla^2_\rho = \lambda_1 + \lambda_2 + \lambda_3 (\lambda_1 \le \lambda_2 \le \lambda_3)$, valuable information regarding stabilizing $\lambda_2 < 0$ and destabilizing $\lambda_2 > 0$) interactions can be obtained. Larger negative values of $sign(\lambda_2)\rho$ indicate stronger interactions, such as hydrogen bonds, whereas values close to zero indicate weaker NCI, such as van der Waals forces. These values reflect both the magnitude and the stabilizing or destabilizing nature of the interactions.

The coordinates of the complexes were obtained from an ensemble of structures at the equilibrium state. These structures were sampled from the production runs and selected using a clustering procedure outlined in a previous publication[23]. The coordinates of the respective binding partners were isolated for further analysis. In order to represent the relevant NCI between MEM_{10}/*MEM* and BTZ/MCP molecules, isosurface volumes were generated. These volumes are proportional to the values of δg^{inter} and are colored based on the range of $sign(\lambda_2)\rho$. For further details, please refer to the following reference[27].

Results and discussion

Characterization of membranes

The effect of water on the membrane has been followed by FTIR analysis; thus, after dipping the membrane in water it can be seen the disappearance of the vibrational band assigned to NCO groups (2270 cm^{-1}) and the concomitant appearance of bands attributed to $-NH_3^+$ groups (1560 cm^{-1}). This can be justified by hydrolysis and protonation of isocyanate groups, as shown in SM, Supplementary Figs. 1–8. NCO hydrolysis led to CO_2 formation, occurring a slightly acidification of media which guarantees the protonation of the amine group. It is also worth highlighting the effect of the CO_2 released on the membrane's surface area. Nitrogen sorption–desorption analysis BET tests with MEM_1 and MEM_5 provided not conclusive results due to the low proportion of NCO groups, but they were elucidative with MEM_{10}. In fact, the active surface area of the MEM_{10} increases twice (from $0.76 \pm 0.05\ m^2\ g^{-1}$ to $1.60 \pm 0.17\ m^2\ g^{-1}$) upon hydrolysis (Fig. 2). Both effects favor sorbate-sorbent interactions since a higher porosity enhance the permeation process of the active ingredient through the membrane making easier to reach the active site and stabilize it as supported by MD simulation. The *WSP*s of the membranes were 63%, 57%, and 57%, for MEM_1, MEM_5 and MEM_{10}, respectively, indicating that an increase in the monomer percentage does not affect the swelling properties of membranes.

The membranes were designed for industrial, agricultural/green-house applications with highly relevant mechanical and thermal properties. In this regard, the membranes *MEM*❶, *MEM*❺, *and MEM*❿ have been tested using a universal testing machine, and Young's modulus values of $1062 \pm 221\ N\ m^{-2}$, $996 \pm 148\ N\ m^{-2}$, and $916 \pm 238\ N\ m^{-2}$ have been obtained, respectively. The elastic modulus slightly decreases as the concentration of the NCO monomer increases since it introduces flexibility, leading to a lower overall stiffness.

From a thermal perspective, the membranes' glass transition temperature (Tg) increases as the mol% of the NCO monomer in the initial material increases (137, 138, and 158 °C for *MEM*❶, *MEM*❺ *and MEM*❿, respectively). This trend is maintained after the hydrolysis of the NCO groups (142, 155, and 170 °C for MEM_1, MEM_5 and MEM_{10}, respectively). This phenomenon is attributed to the incorporation of the NCO or $-NH_3^+$ moieties, which can introduce stronger intermolecular interactions within the membrane structure, resulting in a higher energy barrier for molecular motion and an elevated Tg. The presence of lateral groups containing NH_3^+ motifs also affects the thermograms, where two distinct T_{max} values can be identified. The first peak (around 290 °C) is attributed to the loss of lateral chains ($-O-CH_2-CH_2-NH_3^+$), resulting in a weight loss of 5.8% for MEM_{10} (theoretical calculation: 5.6%). The second T_{max} peak is associated with the main weight loss of the materials, occurring around 410–425 °C (More information in SM, Supplementary Figs. 1–6).

The designed and developed material exhibits suitable mechanical and thermal properties for the intended applications, making it promising for diverse uses.

Table 1 | Performance of membranes for removal of BTZ and MCP and cost analysis; data are means of 2 replicates ± standard deviation

	Bentazon		Mecoprop		*Cost* (€ g^{-1})[a]
	q_e (±*std*) (mg g^{-1})	*RE* (±*std*) (%)	q_e (±*std*) (mg g^{-1})	*RE* (±*std*) (%)	
MEM	0.416 ± 0.01	6.8 ± 0.4	0.222 ± 0.004	4.0 ± 0.1	0.12
MEM_1	5.3 ± 0.1	87 ± 5	4.0 ± 0.1	71 ± 1	0.18
MEM_5	5.8 ± 0.1	94 ± 5	4.5 ± 0.1	80 ± 1	0.42
MEM_{10}	5.7 ± 0.1	94 ± 5	4.2 ± 0.1	76 ± 1	0.72

std standard deviation.
[a]The cost was calculated based on the amount of the chemical used to synthesize 1 g of material.

Removal performance tests of membranes

All assays were conducted in Milli-Q water because we believe that in the initial phases of developing such materials, it is crucial to avoid interactions with salts from buffers, ultimately providing higher-quality information.

The first sorption screening tests have clearly shown the key role of the monomer containing NH_3^+ groups in the sorbent-sorbate interactions (Table 1). The results also demonstrate that an increase in the molar percentage of $-NH_3^+$ does not lead to a significant increase of q_e or *RE* values, in line with, for example, the obtained swelling values. Furthermore, considering a simple cost analysis of the chemicals (€ g^{-1}), the prices for MEM_1, MEM_5 and MEM_{10} increase by 50%, 250%, and 500%, respectively, compared to *MEM*. Based on this evidence, MEM_1 was chosen for further analysis.

Interaction between pesticides and MEM[1]

Sorption and transport studies. Complementary analytical approaches have been used for a deep evaluation of the interaction sorbate-sorbent.

Permeation analysis (Fig. 3a) shows similar D_{ap} values for both pesticides ($\approx 1 \times 10^{-9}\ cm^2\ s^{-1}$), indicating similar affinity. However, time-lag values (θ) for BTZ indicate higher resistance to passing through the membrane, which might be related to its lower solubility in water (more information in Supplementary Table 3). Additionally, the solution of Fick's 2nd law equation fits well to the sorption kinetic data (Fig. 3b), allowing the calculation of effective diffusion and partition coefficients (Supplementary Table 3). The partition coefficients show that both pesticides have a higher affinity towards the membrane phase, suggesting an interaction between pesticides and the polymeric structure or stabilization of active ingredient by hydrophobic media of polymer. Despite of that, an analysis of Fig. 3b shows that at short-range times ($q_t/q_e < 0.6$), a deviation to lower values of experimental data (relative to the fitting line) is observed. By using the power law equation[28] ($q_t/q_e = kt^n$, where k and n are constants, and n characterizes the transport mechanism), it can be concluded that for short-range times, the sorption is non-Fickian, indicating the occurrence of coupling of diffusional and relaxational mechanisms; the latter might be due to interactions between the sorbate and the polymeric chain[29].

Although no conclusions can be drawn about the differences between the sorption of BTZ and MCP into MEM_1 as seen by permeation and sorption kinetics, the same cannot be concluded from the evaluation of sorption isotherms (Fig. 3c). It can readily be noticed that both analytes show different sorption mechanisms. The BTZ isotherm is fitted by the Langmuir model, suggesting an ordered sorption process with a monolayer formation and film saturation with $q_m = 18\ mg\ g^{-1}$. On the other hand,

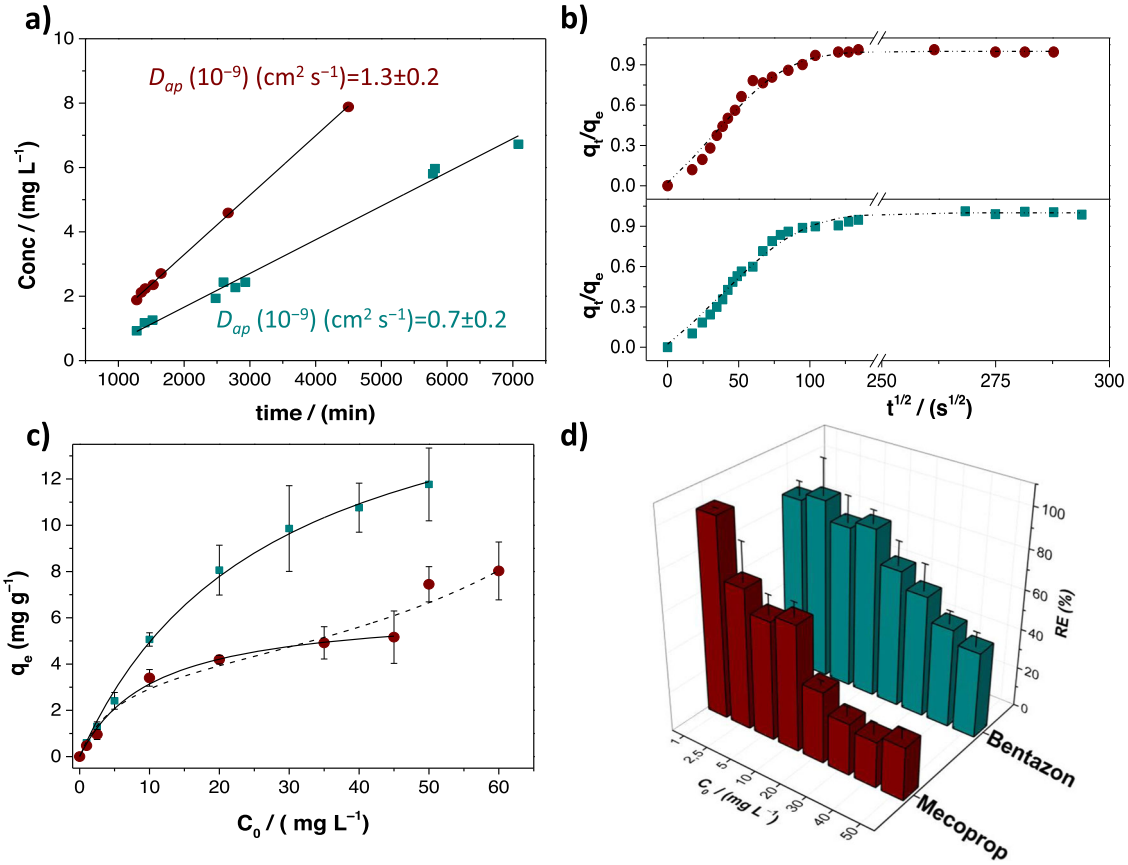

Fig. 3 | Characterization of the interaction of *MEM$_1$* with mecoprop (bordeaus) and bentazon (cyan) in terms of. a Permeation at the steady-state conditions, **b** sorption kinetics, **c** sorption isotherm, and **d** removal efficiency. Details about the meaning of solid and dashed lines are given in the text; data are means of 2 replicates ± standard deviation.

MCP presents a multilayer sorption process represented by the BET model, which means that once the first layer is saturated (q_m = 3.9 mg g^{-1}), the sorbate-sorbate interactions are predominant, achieving a maximum sorption of 112.6 mg L^{-1}. This finding may also justify the higher interaction between MCP-*MEM$_1$* indicated by the previous results and might explain the non-Fickian diffusion process discussed above.

In both cases, the main conclusion of these experiments is that the removal membrane performance increases by decreasing the initial concentrations of pesticides, achieving *RE*s equal to ≈90% and >99% for BTZ and MCP, respectively (Fig. 3d),

NMR and FT-IR studies. The titration of MCP with *POL$_{10}$* by NMR shows the disappearance of the ^{1}H band of the carboxylic acid group on MCP as the amount of *POL$_{10}$* increases, a clear indication of the chemical environmental changes, which may include sorbent-sorbate interactions[30–32]. By calculating the area under the peak at 13 ppm (Fig. 4a), the concentration of MCP remaining at equilibrium, [MCP]$_{eq}$, is computed (Figs. 4a, b). By performing a nonlinear least squares fitting (Fig. 4b - red line), the value of the equilibrium constant $K = 57 \pm 4$ dm^3 mol^{-1} is obtained. Figure 4c illustrates the decrease in [MCP] as *POL$_{10}$* is added, along with the fitting obtained using the aforementioned equation in red. Once the value of K is determined, it is possible to calculate the concentration of all species at equilibrium (Fig. 4c).

Regarding FT-IR (Fig. 4d), the vibrational modes at 2800–3050 cm^{-1} range can be assigned to stretching vibrations of polymer's main chain's methylene groups (-CH_2-). It can be seen that the intensity of bands is dependent on the presence of active ingredients. In fact, by using the ratio of the intensity of peaks at 2950 cm^{-1} (I_1) and 2924 cm^{-1} (I_2) leads to the following values: I_1/I_2 = 1.30, 1.20, and 1.07 for the polymer without and with MCP and BTZ, respectively (Fig. 4d). FTIR results indicate an interaction at level of –CH_2– groups of the aliphatic chains of the monomers constituting the membrane. In summary, the execution of molecular dynamics (MD) studies proves to be of utmost importance to confirm both the type and the active sites of interactions between sorbent and sorbate, as detailed in "Interaction patterns in solution".

Interaction patterns in solution

Table 2 presents a comprehensive overview of the cumulative potential energies observed during the simulations and the corresponding binding enthalpies for the complexes formed between *MEM$_{10}$* and *MEM* with the two pesticides, as well as for the individual hydrated components (*MEM$_{10}$*, *MEM$_{10}$*, BTZ, MCP), and pure water. The results indicate a noteworthy impact of the -NH_3^+ group within *MEM$_{10}$* on the binding affinity towards both pesticides, corroborating previous experimental findings and in silico studies[21].

The complexes that are more strongly favored in enthalpic terms are *MEM$_{10}$*:BTZ (−40 kJ mol^{-1}) and *MEM$_{10}$*:MCP (− 15 kJ mol^{-1}), The ΔH values follow the order *MEM$_{10}$*:BTZ < *MEM$_{10}$*:MCP < *MEM:*BTZ < *MEM:*MCP, suggesting that the most stable complexes are those containing -NH_3^+ side groups. While *MEM$_{10}$*:BTZ and *MEM$_{10}$*:MCP complexes display binding enthalpies within typical range (see ref. 21), the *MEM:*BTZ and *MEM:*MCP complexes display positive values (441 kJ mol^{-1} and 694 kJ mol^{-1}, respectively), suggesting that the association between the two pesticides with *MEM* is very unlikely or unstable when there are no -NH_3^+ side groups in the polymeric structure (see Table 2).

The graphical representation of the average distances between the -NH_3^+ group of *MEM$_{10}$* and the negative groups of BTZ (N^-) and MCP (COO^-) over time (Supplementary Figure 11) provides insights into the

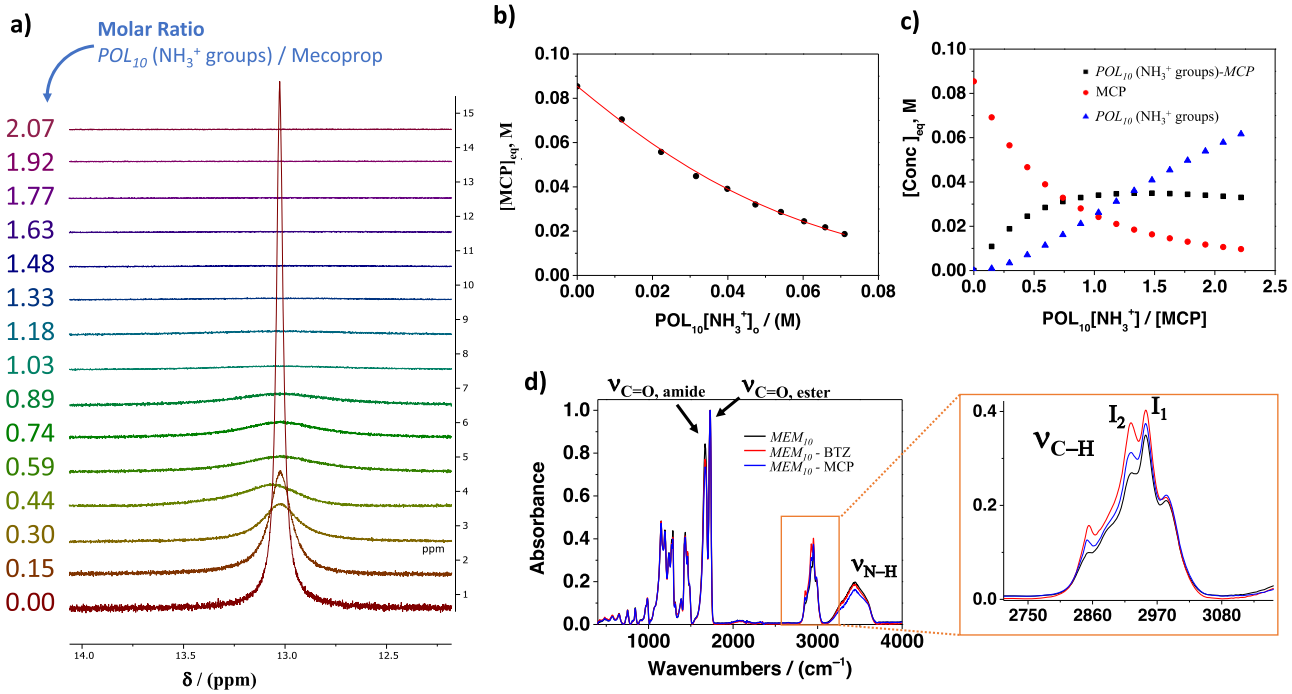

Fig. 4 | Characterization of the interaction of *POL*$_{10}$ with MCP by ^{1}H-NMR, and *MEM*$_{10}$ with MCP and BTZ by FT-IR. a Overlay of ^{1}H-NMR spectra using DMSO-d_6 as solvent; experimental conditions: initial concentration of MCP = 8.5×10^{-2} mol dm^{-3}; *POL*$_{10}$ solution concentration = 225 mg mL^{-1}; volume of each addition = 40 μL. **b** Evolution of the concentration of MCP as the concentration of *POL*$_{10}$ increases. The fitting by least squares is represented in red. **c** Diagram of species in equilibrium. **d** FT-IR spectra of *MEM*$_{10}$ (black line), and of *MEM*$_{10}$ after dipping for 24 h in 208 mol dm^{-3} aqueous solutions of mecoprop (blue line) and bentazon (red line).

spatial arrangement and potential binding patterns between *MEM*$_{10}$ and pesticides. The distance profile of the charged groups in the *MEM*$_{10}$:BTZ complex suggests the presence of multiple conformations upon complex formation and variability in the interaction modes, indicating a more dynamic behavior than the *MEM*$_{10}$:MCP complex. There are two predominant binding modes that will favor the binding enthalpy in *MEM*$_{10}$:BTZ, involving (*i*) the preferential interaction between the -NH_3^+ and N^- groups (<0.5 nm), driven by a stronger electrostatic attraction (see Fig. 5a, top) and by N-H···N type interactions and (*ii*) the presence of an alternative configuration in which the charged groups exhibit a distinct spatial arrangement, resulting in a significant separation between them (>1.0 nm, Supplementary Figure 12) and precluding direct interaction (see Fig. 5a, bottom). Such dynamic behavior can be explained by considering the solvation effects, polymer conformational changes, polymer-pesticide interactions, and binding entropy.

Table 2 | Averaged total potential energies computed for the complexes between *MEM*$_{10}$ and BTZ and MCP in solution and the corresponding binding enthalpies (kJ mol^{-1})

System	Simulation	BTZ Potential energy (kJ mol^{-1})	MCP Potential energy (kJ mol^{-1})
MEM$_{10}$	**Pure Water**	−236,541	−234,793
	***MEM*$_{10}$**	−236,385	−234,638
	Pesticide	−238,702	−235,177
	Complex	−238,586	−235,037
		Binding enthalpy (kJ mol^{-1})	**Binding enthalpy** (kJ mol^{-1})
	Δ*H*	−40	−15
MEM	**Pure Water**	−236,536	−236,294
	MEM	−236,796	−236,554
	Pesticide	−238,495	−236,644
	Complex	−238,314	−236,210
		Binding enthalpy (kJ mol^{-1})	**Binding enthalpy** (kJ mol^{-1})
	Δ*H*	441	694

Solvent effects. The behavior of *MEM*$_{10}$ and each pesticide in solution is strongly influenced by the surrounding water molecules, particularly in explicit solvent simulations. In the *MEM*$_{10}$:BTZ and *MEM*$_{10}$:MCP complexes, the solvation shell formed by water molecules (Supplementary Fig. 12) may prevent direct interactions between the charged group of the polymer and the pesticides, i.e., the water molecules surrounding the -NH_3^+ group of the polymer effectively solvate the charged group (Supplementary Figs. S12 and S13), preventing it from directly interacting with the negative group of the pesticides (-N^- of BTZ and -COO^- in MCP). This behavior is common in aqueous systems, in which water molecules can mediate interactions between charged species[33,34]. The coordination number (rcn) presented in Supplementary Figure 13 represents the average number of water molecules in the immediate vicinity of the -NH_3^+ group of *MEM*$_{10}$ free in solution and upon binding to BTZ and MCP, indicating the degree of hydration. For the *MEM*$_{10}$:BTZ complex, the amount of water molecules in the immediate vicinity of the -NH_3^+ group decreases upon complex formation. The set of rcn curves is delimited above by the -NH_3^+ of *MEM*$_{10}$ in the complex with MCP, which corresponds to a system exhibiting a higher degree of solvation. This observation is consistent with the lower negative binding enthalpy of −15 kJ mol^{-1}, indicating weaker or less favorable interactions between *MEM*$_{10}$ and MCP compared to the *MEM*$_{10}$:BTZ complex ($\Delta H = -40$ kJ mol^{-1}). The correlation between desolvation and binding enthalpy has been highlighted in our previous studies[23,33].

Supplementary Fig. 14a shows that the complex formation between BTZ and MCP leads to a significant depletion of water molecules from the vicinity of both pesticides. Furthermore, from Supplementary Fig. 14b, the slight change in the slope of the rcn curve suggests that MCP does not undergo significant desolvation upon binding to *MEM*.

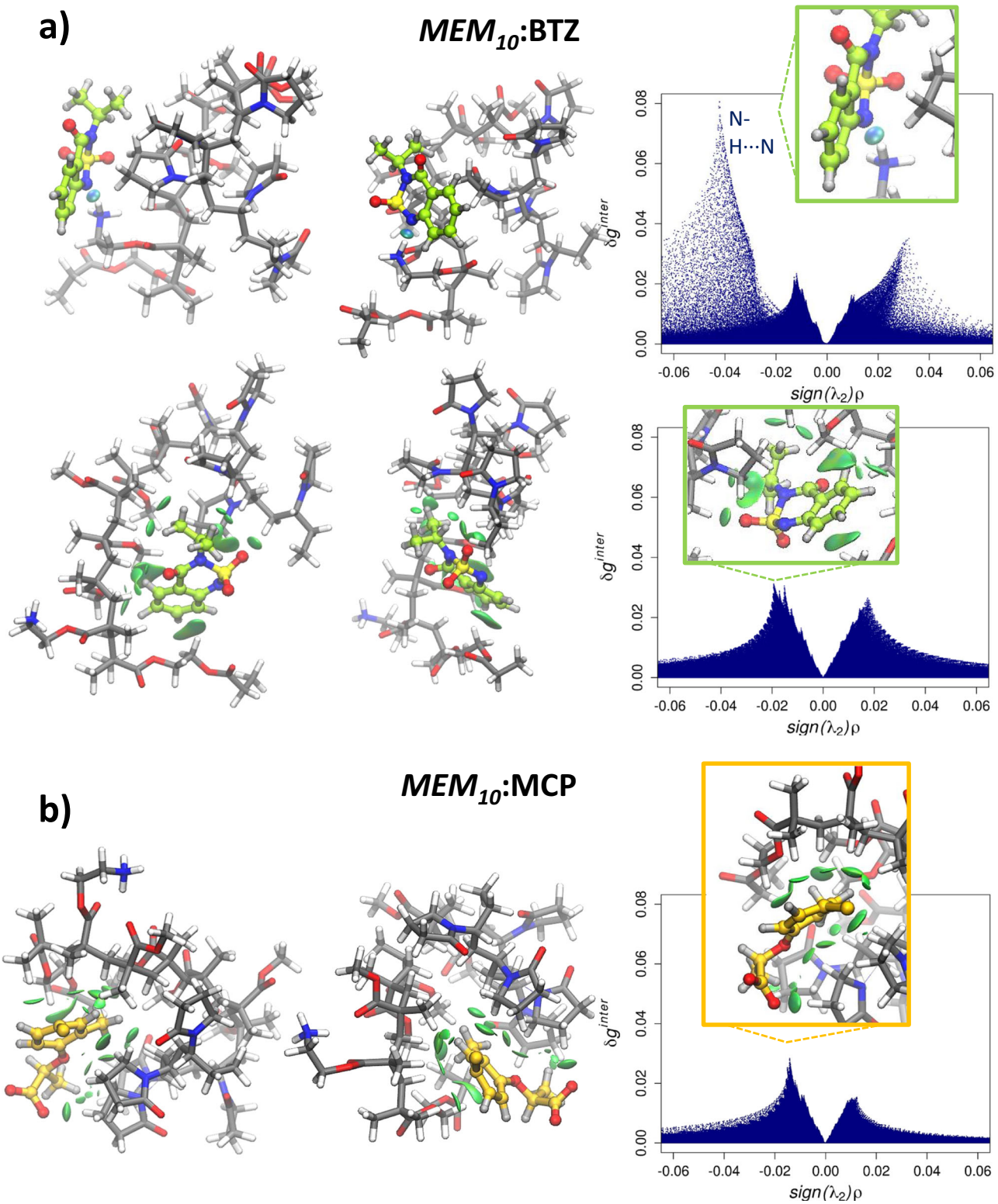

Fig. 5 | Interaction patterns: MEM10-BTZ and MEM10-MCP complexes. a An overview of the interaction patterns between MEM_{10} and BTZ upon complex formation, illustrated by the 3D isosurfaces (right) and 2D scatter plots (left) for two preferential complex configurations. Stabilizing/destabilizing NCI are represented in blue/red and van der Waals forces are colored in green (volume cutoff of $\delta g_{inter} = 0.05$; color coding: $-0.1 \leq sign(\lambda_2)\rho \leq 0.1$). The MEM_{10} backbone is featured in gray as licorice, while BTZ is represented in ball-and-stick and colored in light green. Nitrogen, oxygen, sulfur and hydrogen atoms are represented in blue, red, yellow and white, respectively. **b** 3D isosurfaces (right) and 2D scatter plots for the complex formation between MEM_{10} and MCP. MCP is represented in ball-and-stick and colored in dark yellow.

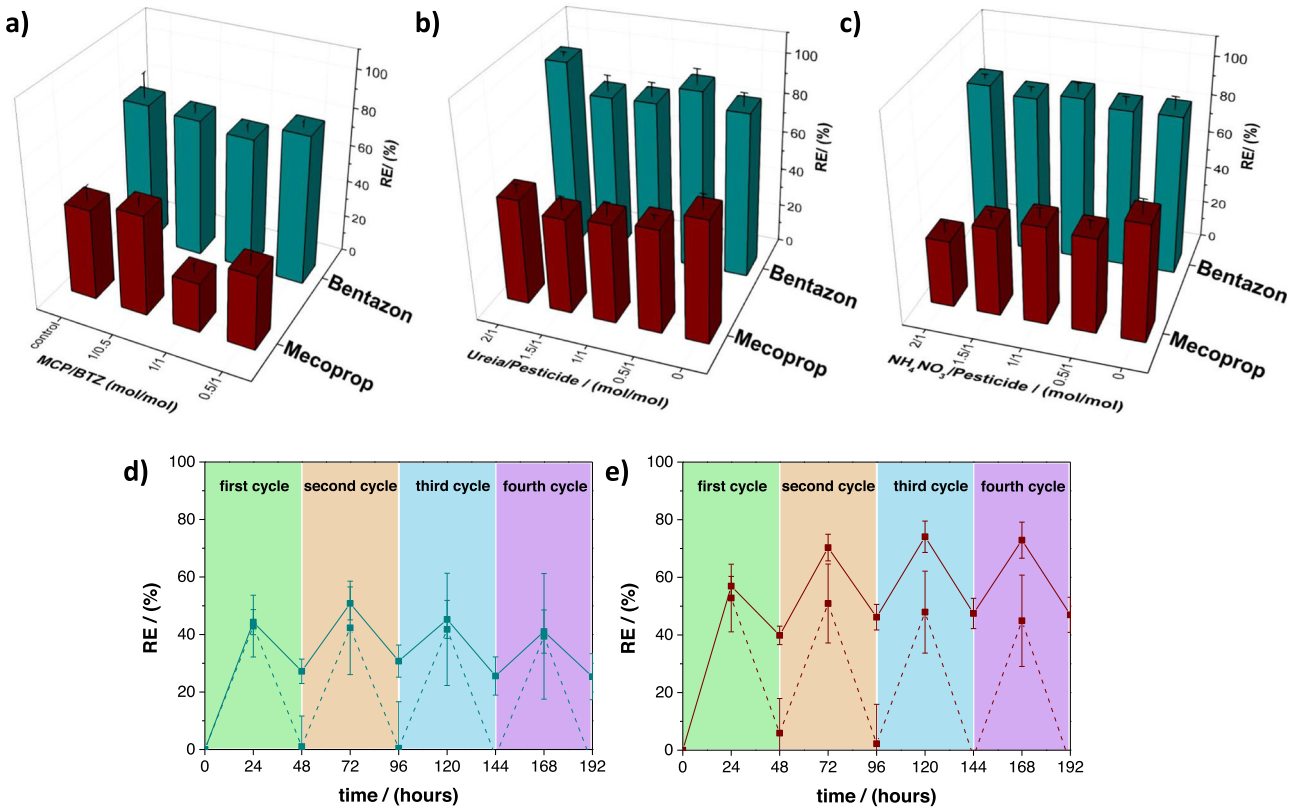

Fig. 6 | Interference and reusability study. Representation of (**a**) competitiveness and selectivity of MEM_1 in the presence of BTZ and MCP; (**b**) and (**c**) interferent analysis in the presence of $CO(NH_2)_2$ and $NH_4^+NO_3^-$, respectively; (**d**) and (**e**) reusability study of MEM_1 washed with ultrapure water (line) and NaOH 0.1 mol dm^{-3} (dashed line) with BTZ (cyan) and MCP (bordeaux), respectively. Data are means of two replicates ± standard deviation.

Polymer conformational changes and polymer-pesticide interactions. In general, the MEM_{10} polymer undergoes dynamic spatial and conformational rearrangements to create a pocket or cavity that accommodates the pesticides and increase complex stability (see Supplementary Figs. S5 and S6). These changes involve adjustments in overall polymer shape and help to optimize the interactions between the polymer and the pesticides, maximizing favorable intermolecular forces such as hydrophobic interactions, Van der Waals forces, or hydrogen bonding. This dynamic conformational behavior allows the polymer to create a favorable environment for the BTZ and MCP molecules, even if there is no direct interaction between the $-NH_3^+$ group of the polymer and the pesticide. It is particularly noteworthy that the MEM_{10}:BTZ complex exhibits a distinct and pronounced alteration of the polymer's conformation, suggesting a stronger response to the presence of BTZ, as confirmed by the significant variation in RMSD values in Supplementary Fig. 15, panels (a) and (d). This could involve rotations or distortions of specific regions of the polymer upon binding.

In one of the most representative binding modes, depicted in Fig. 5a (bottom), there is no direct interaction between the charged groups as the $-NH_3^+$ group remains solvated by water molecules, the polymer adopts a scorpion-like structure around the pesticide[35], creating a favorable environment for the pesticide to reside. This conformational adaptation allows for the stabilization of the MEM_{10}-BTZ interaction, as suggested by the distribution of distances between the centroids of the binding partners (Supplementary Fig. 16), and by the structural difference between the MEM_{10} backbone, free in solution (Supplementary Fig. 15, panel a) and in the presence of BTZ (Supplementary Fig. 16b, d). The formation of a scorpion-like structure around the pesticide may result in a decrease in the overall system entropy. This decrease in entropy arises from the polymer adopting a more ordered structure upon binding. As a result, the RMSD of the MEM_{10} is lower in the bound state compared to its free form in solution (see Supplementary Fig. 15a, b). The propensity of MEM_{10} for folding and unfolding to accommodate BTZ, as depicted in Supplementary Fig. 15a–c, and Supplementary Fig. 17, panels a and b, also contributes to the stabilization of the complex. The complex formation is thus favored by two preferential polymer conformations corresponding to (*i*) a distorted loop in which the $-NH_3^+$ group of the polymer interacts directly with the N^- group of BTZ through a N-H···N hydrogen bond, as shown in Fig. 5a (top) by the 3D isosurface with a blue center and by the large diffuse peak at $sign(\lambda_2)\rho \approx -0.04$, and (*ii*) a scorpion-like loop formed upon complex formation through C-H···π dispersion interactions and a S-H···O type interaction, as illustrated by the large volumes and large peaks in Fig. 5a (bottom), with respective maxima defined at $-0.01 < sign(\lambda_2)\rho < -0.02$. The formation of polymer loops is also confirmed by the smaller end-to-end distances between the terminal methyl groups of the polymers MEM_{10} upon complex formation with BTZ and MCP (Supplementary Fig. 18a).

Although MEM_{10} polymer has the potential to form a C-H···O hydrogen bond with the carboxyl group of MCP and C-H···π dispersion interactions and hydrophobic C-H···C-H interactions (Fig. 5b), bonding involving BTZ is more likely, as indicated by the volumes of the isosurfaces and their associated peak densities. No stable complexes are formed in the presence of the neutral polymer *MEM*, as suggested by the positive ΔH values (Table 2) and by the weak and diffuse interactions (Supplementary Figure 19). These interaction patterns confirm the previous results from the experimental studies and the corresponding estimated binding enthalpies.

Reusability and interference study

Competitiveness tests show that when the MEM_1 is immersed in an equimolar mixture of the two pesticides, the *RE* is higher for BTZ than for MCP (72% vs 27%), denoting a greater affinity for the former (Fig. 6a). In line with these results, the interference study carried out with two of the most applied nitrogen fertilizers, such $NH_4^+NO_3^-$ and $CO(NH_2)_2$, demonstrated that

Table 3 | Figures of merit: a comparative table of some of the most relevant papers in the field

Target	Material	Reusable? (N° cycles)	q_m (mg g^{-1})	*RE*	Observations	Ref.
Bentazon	Nanocrystalline powder of TiO_2	No	n.a.	99	UV radiation is required for the photocatalytic degradation of Bentazone	32
	Grain of Broadleaf P4	No	n.a.	38–73	It is used as granulated compound into wetlands	36
	Powder of calcinated hydrotalcites	Yes (4)	101	50	-	37
	Particles of magnetic ion exchange resin	No	n.a.	≈99	Exchange resin	31
	Activated carbon powder-CAT	No	392	n.a.	-	38
	Activated carbon powder-CARBOPAL	No	185	n.a.	-	
	Polyimide membrane	Yes (3)	n.a.	89	Used as a filtration membrane	39
	Phenolic resin	Yes (3)	129	n.a.		40
	Calcinated phenolic resin		175	n.a.		
	Powder of two-line ferrihydrite	No	309	n.a.	-	41
	MEMu Membrane	Yes (4)	12	95	-	This study
Mecoprop	Powder of activated carbon	No	n.a.	≈80	It is used in wastewater treatment by adding the powder.	42
	Granulated activated carbon	No	20.	99	-	43
	Spruce biochar	No	n.a.	<20		
	Powder of calcinated hydrotalcites	Yes (4)	300	≈95	-	44
	Powder of two-line ferrihydrite	No	740	n.a.	-	41
	MEMu Membrane	Yes (4)	8	>99	-	This study

BTZ is not affected under the chosen working conditions, actually with no-ionic urea it was observed an enhancement of the *RE* at 97% at molar ratio BTZ:fertilizer 1:2. On the other hand, MCP sorption is affected by the presence of both interferent with a decrease of 17 and 42% of the *RE* with urea and ammonium nitrate, respectively (Figs. 6b, c). The higher interaction with BTZ can be explained by the MD results that indicate two types of interactions with the membrane which contribute to greater stabilization of the system MEM_1:BTZ.

Finally, the reuse tests were performed by washing the membrane in ultrapure water and in NaOH 0.1 mol dm^{-3}, demonstrating that the material is reusable at least 4 times. In particular, it can be noticed that the washing step with water only grants a partial release of about 50% of MCP or BTZ; however, for MCP, it registered an enhancement of 23% on the subsequent sorption cycles (Fig. 6d). We attribute this to a slight pH change induced by MCP in the material, as we are working in a non-buffered environment, which stabilizes from the second cycle onwards. Differently, the washing steps with NaOH 0.1 mol dm^{-3} permit a total release of both active ingredients, maintaining unchanged the sorption performance of the membrane (Fig. 5e). The analysis was performed in duplicates.

Comparison with other studies. Table 3 summarizes the most relevant papers in the field in recent years, in terms of type of material, removal efficiency and capacity and reusability.

Although several materials have the capacity to remove BTZ or MCP, they do so under complex conditions that make their implementation in real-world tests difficult. Most of these materials are powders or resins that are challenging to extract from the medium. Furthermore, while many of these materials have high removal capacity values, their efficiencies were obtained by using pesticide concentrations well above the legal limits, reaching values ranging from 20 to 99%. Our membrane, under depicted experimental conditions, demonstrates its peak efficacy in pesticide removal as their concentrations diminish (95% for BTZ and >99% for MCP). Furthermore, it is crucial to underscore that only a limited number of these materials can sustain repeated usage, and our material underwent testing for 4 cycles without any degradation in performance, thus presenting a significant advancement in this domain.

Discussion

In this study, we have successfully developed reusable polyacrylic membranes specifically designed to efficiently remove two widely used pesticides, mecoprop and bentazon. These membranes exhibit notable properties such as ease of handling, durability, and reusability, providing a practical and environmentally friendly solution for water and soil remediation. We have extensively evaluated the membrane composition, properties, and interactions with the target pesticides using comprehensive characterization techniques including NMR, TGA, DSC, mechanical testing, N2 adsorption, and FTIR analysis. Sorption kinetics studies, isotherms, and permeation studies provided valuable insights into the underlying sorption mechanisms, with a consistent removal efficiency >95% over at least four reuse cycles, and permeability coefficients for these pesticides. Furthermore, through molecular dynamics simulations and NMR analysis, we have unveiled intricate molecular-level interactions between the pesticides and the polymeric membranes, revealing the scorpion-like conformation of the macromolecular chains surrounding the pesticides. This study lays the groundwork for widespread adoption of reusable polyacrylic membranes in pesticide extraction, offering sustainable and effective strategies for remedying pesticide contamination in water sources.

Supplementary material

Characterization of polymers by FT-IR, NMR, TGA and DSC; calibration curves by UV–Vis of bentazon and mecoprop; study of the interaction between POL_{10} and MCP by ^{1}H-NMR; transport and sorption parameters for bentazon and mecoprop using MEM_1; additional information to the in-silico study.

Data availability

The raw data required to reproduce these findings are available to download from https://riubu.ubu.es/handle/10259/5684 (Dataset of the work "UBU-Polymers Research Group 27022024").

Received: 5 September 2023; Accepted: 13 April 2024;
Published online: 14 May 2024

References

1. Holland, P. T. Pesticides report 36. Glossary of terms relating to pesticides (IUPAC Recommendations 1996). *Pure Appl. Chem.* **68**, 1167–1193 (1996).
2. Knowles, A. Recent developments of safer formulations of agrochemicals. *Environmentalist* **28**, 35–44 (2008).
3. Brusseau, M. L. & Chorover, J. Chemical processes affecting contaminant transport and fate. in Environmental and Pollution Science 113–130 (Academic Press, 2019).
4. Barzman, M. et al. Eight principles of integrated pest management. *Agron. Sustain. Dev.* **35**, 1199–1215 (2015).
5. Wagner, S. C., Zablotowicz, R. M., Gaston, L. A., Locke, M. A. & Kinsella, J. Bentazon degradation in soil: Influence of tillage and history of bentazon application. *J. Agric. Food Chem.* **44**, 1593–1598 (1996).
6. McDuffie, H. H. et al. Non-Hodgkin's lymphoma and specific pesticide exposures in men: cross-Canada study of pesticides and health. *Cancer Epidemiol. Biomark. Prev.* **10**, 1155–1163 (2001).
7. Fang, Y. et al. Leaf proteome analysis provides insights into the molecular mechanisms of bentazon detoxification in rice. *Pestic. Biochem. Physiol.* **125**, 45–52 (2015).
8. Gluhar, S., Kaurin, A., Grubar, T., Prosen, H. & Lestan, D. Dissipation of mecoprop-P, isoproturon, bentazon and S-metolachlor in heavy metal contaminated acidic and calcareous soil before and after EDTA-based remediation. *Chemosphere* **237**, 124513 (2019).
9. Béranger, R. et al. Multiple pesticides in mothers' hair samples and children's measurements at birth: Results from the French national birth cohort (ELFE). *Int. J. Hyg. Environ. Health* **223**, 22–33 (2020).
10. Barbieri, M. V. et al. Evaluation of the occurrence and fate of pesticides in a typical Mediterranean delta ecosystem (Ebro River Delta) and risk assessment for aquatic organisms. *Environ. Pollut.* **274**, 115813 (2020).
11. Kuster, M. et al. Analysis of 17 polar to semi-polar pesticides in the Ebro river delta during the main growing season of rice by automated on-line solid-phase extraction-liquid chromatography–tandem mass spectrometry. *Talanta* **75**, 390–401 (2008).
12. Loos, R. et al. EU-wide monitoring survey on emerging polar organic contaminants in wastewater treatment plant effluents. *Water Res.* **47**, 6475–6487 (2013).
13. Guirado-Moreno, J. C. et al. Democratization of copper analysis in grape must following a polymer-based lab-on-a-chip approach. *ACS Appl. Mater. Interfaces* **15**, 16055–16062 (2023).
14. Vallejos, S. et al. Putting to work organic sensing molecules in aqueous media: Fluorene derivative-containing polymers as sensory materials for the colorimetric sensing of cyanide in water. *Chem. Commun.* **46**, 7951–7953 (2010).
15. Bustamante, S. E. et al. Polymer films containing chemically anchored diazonium salts with long-term stability as colorimetric sensors. *J. Hazard. Mater.* **365**, 725–732 (2019).
16. Valente, A. J. M., Polishchuk, A. Y., Lobo, V. M. M. & Burrows, H. D. Transport properties of concentrated aqueous sodium dodecyl sulfate solutions in polymer membranes derived from cellulose esters. *Langmuir* **16**, 6475–6479 (2000).
17. West, P. C., Biggs, R., McKenney, B. A. & Monfreda, C. Feeding the World and Protecting Biodiversity. in Encyclopedia of Biodiversity (ed. Levin A. S.) vol. 3 426–434 (Elsevier, 2013).
18. Finch, H. J. S., Samuel, A. M. & Lane, G. P. F. Fertilisers and manures. in Lockhart & Wiseman's Crop Husbandry Including Grassland (eds. Finch, H. J. S., Samuel, A. M. & Lane, G. P. F.) 63–91 (Elsevier, 2014).
19. MolGpKa. https://xundrug.cn/molgpka.
20. Utzeri, G., Cova, T. F., Murtinho, D., Pais, A. A. C. C. & Valente, A. J. M. Insights on macro- and microscopic interactions between Confidor and cyclodextrin-based nanosponges. *Chem. Eng. J.* **455**, 140882 (2023).
21. Cova, T. F. G. G., Milne, B. F., Nunes, S. C. C. & Pais, A. A. C. C. Drastic stabilization of junction nodes in supramolecular structures based on host–guest complexes. *Macromolecules* **51**, 2732–2741 (2018).
22. Jakalian, A., Jack, D. B. & Bayly, C. I. Fast, efficient generation of high-quality atomic charges. AM1-BCC model: II. Parameterization and validation. *J. Comput. Chem.* **23**, 1623–1641 (2002).
23. Cova, T. F., Milne, B. F. & Pais, A. A. C. C. Host flexibility and space-filling in supramolecular complexation of cyclodextrins: a free-energy-oriented approach. *Carbohydr. Polym.* **205**, 42–54 (2019).
24. Lin, Z. & van Gunsteren, W. F. Refinement of the application of the GROMOS 54A7 force field to β-peptides. *J. Comput. Chem.* **34**, 2796–2805 (2013).
25. Cova, T. F. G. G., Nunes, S. C. C., Pinho e Melo, T. M. V. D. & Pais, A. A. C. C. Bambusurils as effective ion caging agents: Does desolvation guide conformation? *Chem. Phys. Lett.* **672**, 89–96 (2017).
26. Lefebvre, C., Khartabil, H. & Boisson, J. The independent gradient model: a new approach for probing strong and weak interactions in molecules from wave function calculations. *ChemPhysChem* **19**, 724–735 (2018).
27. Lefebvre, C., Khartabil, H., Boisson, J., Contreras-garcı, J. & He, E. Accurately extracting the signature of intermolecular interactions present in the NCI electron density †. *PCCP* **19**, 17928–17936 (2017).
28. Crank, J. The Mathematics of Diffusion. (Clarendon Press Oxford, 1975).
29. Polishchuk, A. & Zaikov, G. Multicomponent Transport in Polymer Systems for Controlled Release. (Gordon Breach Sci. Pub., 1997).
30. Azzali, A., d'Agostino, S. & Grepioni, F. Tuning the solubility of the herbicide bentazon: from salt to neutral and to inclusion complexes. *ACS Sustain Chem. Eng.* **9**, 12530–12539 (2021).
31. Liu, Z. et al. Removal of bentazone from micro-polluted water using MIEX resin: Kinetics, equilibrium, and mechanism. *J. Environ. Sci.* **23**, 381–387 (2011).
32. Pourata, R., Khataee, A. R., Aber, S. & Daneshvar, N. Removal of the herbicide Bentazon from contaminated water in the presence of synthesized nanocrystalline TiO2 powders under irradiation of UV-C light. *Desalination* **249**, 301–307 (2009).
33. Cova, T. F. G. G., Nunes, S. C. C. & Pais, A. A. C. C. Free-energy patterns in inclusion complexes: the relevance of non-included moieties in the stability constants. *Phys. Chem. Chem. Phys.* **19**, 5209–5221 (2017).
34. Schiebel, J. et al. Intriguing role of water in protein-ligand binding studied by neutron crystallography on trypsin complexes. *Nat. Commun.* **9**, 3559 (2018).
35. Djordjevic, J., Barch, M. & Uhrich, K. E. Polymeric micelles based on amphiphilic scorpion-like macromolecules: novel carriers for water-insoluble drugs. *Pharm. Res.* **22**, 24–32 (2005).
36. Jing, Y. et al. Superabsorbent polymer as a supplement substrate of constructed wetland to retain pesticides from agricultural runoff. *Water Res.* **207**, 117776 (2021).
37. Pérez, A., Otero, R., Romero Esquinas, A., Jiménez, J. R. & Fernández, J. M. Potential use of modified hydrotalcites as adsorbent of Bentazon and Metazachlor. *Appl. Clay Sci.* **141**, 300–307 (2017).
38. Spaltro, A. et al. Adsorption of bentazon on CAT and CARBOPAL activated carbon: experimental and computational study. *Appl. Surf. Sci.* **433**, 487–501 (2018).
39. Ali, J. et al. A mixed matrix polyimide ultrafiltration membrane for efficient removal of bentazon from water. *Chem. Eng. J.* **433**, 134596 (2022).
40. Otero, R. et al. Mesoporous phenolic resin and mesoporous carbon for the removal of S-Metolachlor and Bentazon herbicides. *Chem. Eng. J.* **251**, 92–101 (2014).

41. Clausen, L. & Fabricius, I. Atrazine, isoproturon, mecoprop, 2,4-D, and bentazone adsorption onto iron oxides. *J. Environ. Qual.* **30**, 858–869 (2001).
42. Bonvin, F., Jost, L., Randin, L., Bonvin, E. & Kohn, T. Super-fine powdered activated carbon (SPAC) for efficient removal of micropollutants from wastewater treatment plant effluent. *Water Res.* **90**, 90–99 (2016).
43. McGinley, J. et al. Batch adsorption of herbicides from aqueous solution onto diverse reusable materials and granulated activated carbon. *J. Environ. Manag.* **323**, 116102 (2022).
44. Otero, R., Fernández, J. M., González, M. A., Pavlovic, I. & Ulibarri, M. A. Pesticides adsorption–desorption on Mg–Al mixed oxides. Kinetic modeling, competing factors and recyclability. *Chem. Eng. J.* **221**, 214–221 (2013).

Acknowledgements

We gratefully acknowledge the financial support provided by all funders. The financial support provided by Fondo Europeo de Desarrollo Regional-European Regional Development Fund (FEDER, ERDF) and Regional Government of Castilla y León -Consejería de Educación, Junta de Castilla y León- (BU025P23) is gratefully acknowledged. This work was supported by the Regional Government of Castilla y León (Junta de Castilla y León) and by the Ministry of Science and Innovation MICIN and the European Union *NextGenerationEU* PRTR. J.M.G. received grant PID2020-113264RB-I00 funded by MCIN/AEI/ 10.13039/501100011033 and by "ERDF A way of making Europe". S.V. received grant BG22/00086 funded by Spanish Ministerio de Universidades. The authors also acknowledge Fundação para a Ciência e a Tecnologia (FCT), the Portuguese Agency for Scientific Research for the financial support through project UIDP/00313/2020. T.C. acknowledges the Junior Researcher Grant CEECIND/00915/2018 assigned by FCT. G.U. thanks FCT for the PhD grant SFR/BD/146358/2019.

Author contributions

Gianluca Utzeri: Methodology, Conceptualization, Validation, Investigation, Final approval of the completed version. José Carlos Guirado-Moreno: Methodology, Conceptualization, Validation, Investigation, Final approval of the completed version. Tânia F. G. G. Cova: Methodology, Validation, Formal analysis, Investigation, Final approval of the completed version. Alberto A.A.C. Pais: Formal analysis, Investigation, Final approval of the completed version. Luis A. E. Batista de Carvalho: Validation, Investigation, Writing - Original Draft, Resources, Supervision, Final approval of the completed version. Saturnino Ibeas: Validation, Review & Editing, Supervision, Final approval of the completed version. José M. García: Conceptualization, Methodology, Writing—Review & Editing, Supervision, Funding acquisition, Final approval of the completed version. Artur J. M. Valente: Writing—Original Draft, Writing—Validation, Final approval of the completed version. Saul Vallejos: Conceptualization, Funding acquisition, Project administration, Methodology, Investigation, Writing—Original Draft, Writing - Review & Editing, Supervision, Final approval of the completed version.

Competing interests

The authors declare no competing interests.

Additional information

Supplementary information The online version contains supplementary material available at https://doi.org/10.1038/s41545-024-00328-3.

Correspondence and requests for materials should be addressed to Artur J. M. Valente or Saúl Vallejos.